



# Canine prostatic cancer cell line (LuMa) with osteoblastic bone metastasis

Said M. Elshafae PhD<sup>1,2,3</sup> | Wessel P. Dirksen PhD<sup>1,4</sup> |  
 Aylin Alasonyalilar-Demirer PhD<sup>1,5</sup>  | Justin Breitbach DVM<sup>1</sup> | Shiyu Yuan BS<sup>6</sup> |  
 Noriko Kantake PhD<sup>6</sup> | Wachiraphan Supsavhad DVM, PhD<sup>7</sup> | Bardes B. Hassan PhD<sup>1,8</sup> |  
 Zayed Attia MS<sup>1,9</sup> | Lucas B. Alstadt BS<sup>1</sup> | Thomas J. Rosol DVM, PhD, MBA<sup>6</sup> 

<sup>1</sup>Department of Veterinary Biosciences, College of Veterinary Medicine, The Ohio State University, Columbus, Ohio

<sup>2</sup>Department of Pathology, Faculty of Veterinary Medicine, Benha University, Benha, Egypt

<sup>3</sup>Department of Neuroscience and Pharmacology, Carver College of Medicine, University of Iowa, Iowa City, Iowa

<sup>4</sup>Department of Veterinary Clinical Sciences, College of Veterinary Medicine, The Ohio State University, Columbus, Ohio

<sup>5</sup>Department of Pathology, Faculty of Veterinary Medicine, Bursa Uludag University, Bursa, Turkey

<sup>6</sup>Department of Biomedical Sciences, Heritage College of Osteopathic Medicine, Ohio University, Athens, Ohio

<sup>7</sup>Department of Pathology, Faculty of Veterinary Medicine, Kasetsart University, Bangkok, Thailand

<sup>8</sup>Department of Pathology, Faculty of Veterinary Medicine, Cairo University, Giza, Egypt

<sup>9</sup>Department of Animal Medicine and Infectious Diseases, Faculty of Veterinary Medicine, Sadat City University, Sadat City, Egypt

## Correspondence

Thomas Rosol, DVM, PhD, Department of Biomedical Sciences, Heritage College of Osteopathic Medicine, 1 Ohio University, 225 Irvine Hall, Athens, OH 45701.  
 Email: [rosolt@ohio.edu](mailto:rosolt@ohio.edu)

## Abstract

**Background:** Osteoblastic bone metastasis represents the most common complication in men with prostate cancer (PCa). During progression and bone metastasis, PCa cells acquire properties similar to bone cells in a phenomenon called osteomimicry, which promotes their ability to metastasize, proliferate, and survive in the bone microenvironment. The mechanism of osteomimicry resulting in osteoblastic bone metastasis is unclear.

**Methods:** We developed and characterized a novel canine prostatic cancer cell line (LuMa) that will be useful to investigate the relationship between osteoblastic bone metastasis and osteomimicry in PCa. The LuMa cell line was established from a primary prostate carcinoma of a 13-year old mixed breed castrated male dog. Cell proliferation and gene expression of LuMa were measured and compared to three other canine prostatic cancer cell lines (Probasco, Ace-1, and Leo) in vitro. The effect of LuMa cells on calvaria and murine preosteoblastic (MC3T3-E1) cells was measured by quantitative reverse-transcription polymerase chain reaction and alkaline phosphatase assay. LuMa cells were transduced with luciferase for monitoring in vivo tumor growth and metastasis using different inoculation routes (subcutaneous, intratibial [IT], and intracardiac [IC]). Xenograft tumors and metastases were evaluated using radiography and histopathology.

**Results:** After left ventricular injection, LuMa cells metastasized to bone, brain, and adrenal glands. IT injections induced tumors with intramedullary new bone formation. LuMa cells had the highest messenger RNA levels of osteomimicry genes (*RUNX2*, *RANKL*, and *Osteopontin* [OPN]), *CD44*, *E-cadherin*, and *MYOF* compared to Ace-1, Probasco, and Leo cells. LuMa cells induced growth in calvaria defects and modulated gene expression in MC3T3-E1 cells.

**Conclusions:** LuMa is a novel canine PCa cell line with osteomimicry and stemness properties. LuMa cells induced osteoblastic bone formation in vitro and in vivo. LuMa PCa cells will serve as an excellent model for studying the mechanisms of osteomimicry and osteoblastic bone and brain metastasis in prostate cancer.

## KEYWORDS

bone, canine, dog, metastasis, osteoblast, prostate cancer, tumor

## 1 | INTRODUCTION

Prostate cancer (PCa) is the most common malignant tumor and the second greatest cause of cancer-related death in men after lung cancer in Western countries. One of the most frequent complications in PCa patients is bone metastasis, which is most often osteoblastic (bone-inducing). Some tumor cells that undergo skeletal metastasis gain features that are usually restricted to bone cells, especially osteoblasts, and this process has been termed osteomimicry.<sup>1-3</sup> Acquiring osteoblastic properties by cancer cells promotes their survival and growth.<sup>4</sup> In addition, some neoplastic cells at their primary site have acquired osteomimicry and this promotes their metastasis to bone. The timing and mechanisms of osteomimicry acquisition are not well understood.

Previous studies have shown that several factors including RANKL, insulin-like growth factor 1 (IGF-1), bone morphogenetic protein 2 (BMP-2), and transforming growth factor beta (TGF $\beta$ ) were involved in acquiring an osteomimicry phenotype in prostate cancer.<sup>5,6</sup> These factors activate intracellular signaling molecules such as Wnt, nuclear factor  $\kappa$ B (NF- $\kappa$ B), and Twist that consequently promote the osteogenic program in PCa cells.<sup>7-11</sup> RANKL-RANK is an important signaling pathway that activates several transcription factors that have a role in multiple processes, including osteomimicry (Sox2, HIF1 $\alpha$ , and Sox9), epithelial-to-mesenchymal transition (EMT and Twist1), neuroendocrine differentiation (FoxA2, Sox9, and HIF1 $\alpha$ ) and stem cell properties (Nanog and Sox2).<sup>12</sup> Some prostate and breast cancer cells mimic the osteoblast phenotype by expressing bone matrix factors such as, OPN,<sup>13,14</sup> osteocalcin (OC)<sup>15</sup> and bone sialoproteins.<sup>13,16-18</sup> In addition, cancer cells can express alkaline phosphatase (ALP)<sup>18</sup> and Runt-related transcription factor 2 (Runx2) proteins, which are important osteoblastic markers.<sup>19</sup>

Runx2 signaling is important in the regulation of bone homeostasis and development. Knockout of *RUNX2* led to early prenatal mortality in mice due to the lack of osteoblast differentiation.<sup>20</sup> Runx2 plays a role in mammary tumorigenesis by increasing proliferation and inhibition of apoptosis in mammary acini.<sup>21</sup> Runx2 also directly induces genes associated with angiogenesis, invasiveness and metastasis including *OPN*, *vascular endothelial growth factor* (VEGF), and *matrix metalloproteinase 9* (MMP-9), and promotes EMT of primary cancers.<sup>21-23</sup> Upregulation of *RUNX2* was accompanied by the increase in Gleason score and metastasis that occurred in prostate cancer.<sup>22,24</sup> Furthermore, Runx2 enhanced growth and migration and promoted osteolytic activity of breast cancer. The messenger RNA (mRNA) expression level of *RUNX2* was shown to be greater in the metastatic human prostatic cell line, PC3, compared to less-metastatic cells lines (LNCaP, C4-2B, and RWPE).<sup>25</sup>

Metastatic cancer cells interact with osteoclasts and osteoblasts in bone to stimulate their activity and disturb the normal balance of bone remodeling. The imbalance may promote an osteosclerotic/osteoblastic response, as in PCa, or an osteolytic process, as in multiple myeloma and breast cancer. The interactions between PCa cells and bone cells and the PCa vicious cycle are not completely understood. To improve our understanding of the mechanism of skeletal metastasis in prostate cancer and the interaction between PCa and the bone microenvironment, animal models of skeletal metastasis using well

characterized cell lines were developed.<sup>21,23,24,26</sup> Few cancer and tumor cell lines have been developed that recapitulate the osteoblastic nature of PCa. These include Ace-1, Probasco, LuCAP-23.1, and MDA-PCa 2a & b.<sup>27-33</sup> In this study, we have established and characterized a novel canine prostatic cell line (LuMa) that has unique osteomimicry properties, stem cell and invasive characteristics, and induces osteoblastic bone metastases in nude mice. These properties demonstrate that LuMa cells will be a valuable model in prostate cancer research.

## 2 | MATERIALS AND METHODS

### 2.1 | Cell lines, calvaria, and frozen tissues

Frozen samples of dog normal prostates (N = 2), benign prostate hyperplasia (N = 2), and primary prostatic cancers (OC, CB, Probasco, and LuMa) were obtained from The Ohio State University (OSU) College of Veterinary Medicine Biospecimen Repository. Calvaria were removed from 5 to 12-day old nude mouse pups (NCR-nu/nu) supplied by the OSU Comprehensive Cancer Center (OSUCCC) Target Validation Shared Resource (TVSR). Four canine prostate cancer cell lines were used in this study including Ace-1,<sup>27</sup> Probasco,<sup>33</sup> Leo,<sup>34</sup> and LuMa (available from ABM Inc, Vancouver, Canada).

### 2.2 | Establishment and validation of canine prostate carcinoma cell line (LuMa)

A sample of fresh cancer tissue (about a 1 cm<sup>3</sup> antemortem biopsy) was removed from a primary prostate carcinoma of a 13-year old mixed breed male castrated dog the day before euthanasia and subsequent necropsy. The tumor tissue was washed 3 $\times$  with sterile Dulbecco phosphate-buffered saline (DPBS) and minced into small pieces ( $\leq 1$  mm<sup>3</sup>) with a sterile scalpel. The pieces were cultivated in Dulbecco's modified Eagle medium (DMEM)/F12 medium supplemented with 20% fetal bovine serum (FBS) (only for the first 2 weeks) or 10% FBS (in the remaining weeks) and 1% penicillin/streptomycin (100 unit/mL penicillin and 100  $\mu$ g/mL streptomycin) in a 75 cm<sup>2</sup> tissue culture flask. The medium was replaced every other day in the first 2 weeks and every 3 days afterward. Differential trypsinization with 0.25% trypsin/ethylenediamine-tetra acetic acid (EDTA) was used for 10 to 30 seconds before medium change to remove stromal cell contamination. The epithelial cells were allowed to become 70% to 90% confluent before passaging. LuMa cells (1  $\times 10^6$ ) passage 78 were submitted to IDEXX BioResearch (Columbia, MO) to perform short tandem repeat (STR) DNA profiling and multiplex PCR analysis for detection of any cross contamination or misidentification.

### 2.3 | Lentiviral luciferase transduction

LuMa cells (100 000) were cultivated with DMEM/F12, 10% FBS, and 1% penicillin/streptomycin (culture medium) in a six-well plate.

Once LuMa cells were approximately 90% to 95% confluent, the medium was replaced with 100  $\mu$ L of luciferase-containing virus (VC 2192 ConcpLuc [VSV-G]),<sup>33</sup> 1.5 mL of DMEM/F12 culture medium, and 1.6  $\mu$ L of polybrene stock (8  $\mu$ g/mL). The plate was centrifuged at 2700 rpm for 1 hour at 30°C and incubated at 37°C and 5% CO<sub>2</sub> for 48 hours after which the virus-containing medium was removed and replaced with culture medium. After 48 hours the cells were evaluated for bioluminescence using an IVIS 100 (Caliper Life Sciences, Hopkinton, MA) and photon signal intensity was quantified using Living Image software version 2.50 (Caliper Life Sciences). Luciferase transfected LuMa cells were trypsinized and cultivated in T75 tissue culture flasks.

## 2.4 | In vitro growth rate

LuMa cells (passage 15) were seeded in six-well culture plates in triplicate. LuMa cells were trypsinized and harvested at days 1, 3, and 5. The cell number, size, and viability were counted using an automated cell counter (Nexcelom Bioscience, Lawrence, MA) and trypan-blue dye exclusion to differentiate between live and dead cells. The doubling time was calculated using the following formula: doubling time = duration (hours)  $\times$  log (2)/[log (final concentration) – log (initial concentration)].

## 2.5 | RNA extraction and quantitative reverse-transcription polymerase chain reaction (qRT-PCR)

RNA was extracted from canine prostatic cancer cell lines (LuMa, Probasco, Ace-1, and Leo), benign prostatic hyperplasia (BPH), normal canine prostate tissues, murine MC3T3 E1 cells  $\pm$  LuMa conditioned media and LuMa cells  $\pm$  mouse calvaria using the QuickGene RNA Extraction Kit (AutoGen, Holliston, MA, Cat. No. FK-RC-S2). Reverse-transcription (RT) of total RNA was performed using the Superscript II First Strand cDNA synthesis kit (Invitrogen). Quantitative RT polymerase chain reaction (PCR) was performed for the reference gene, glyceraldehyde 3-phosphate dehydrogenase (GAPDH) for LuMa cells, and ubiquitin C (UBC) for MC3T3-E1 cells, as well as for the osteomimicry, stemness, and prostate cancer progression and metastasis genes including myoferlin (MYOF), runt-related transcription factor 2 (RUNX2), snail homolog 1 (SNAIL), RANKL, SPP1 (osteopontin, OPN), E-cadherin, TWIST, VIMENTIN, androgen receptor (AR), calcium-sensing receptor (CaR), folate hydrolase (FOLH1 or PSMA), TGF $\beta$ , CD44, and CD133 (PROMININ) using canine-specific primers (Table 1). qRT-PCR was completed for the following genes in MC3T3-E1 cells; OPG (osteoprotegerin), RANKL, OPN, OC and RUNX2. For testing primer specificity, all qRT-PCR products were verified by electrophoresis on a 2% agarose gel and stained with ethidium bromide to confirm a single amplification product of the expected size. Sequences were verified by a BLAST search using the NCBI website.

## 2.6 | Induction of osteoblast differentiation

Murine preosteoblast cells, MC3T3-E1 (ATCC, Manassas, Virginia) (200 000 cells), were cultivated in six (25 cm<sup>2</sup>) flasks and cultured for 2 days in  $\alpha$ -minimum Eagle medium ( $\alpha$ -MEM) supplemented with 10% FBS and 1% penicillin/streptomycin. On day 3, the media were replaced in three flasks with  $\alpha$ -MEM medium preincubated with LuMa cells (LuMa condition medium [CM]) for 48 hours. Photographs of MC3T3-E1 cells were taken at day 5 of the experiment using a Nikon 300 Diaphot inverted microscope supplied with a Tucsen camera. To confirm the differentiation of MC3T3-E1 cells, ALP activity assay (Anaspec, Fremont, CA) and qRT-PCR of osteogenic-related genes (OPN and OC) were performed for the MC3T3-E1 cells.

## 2.7 | Coculture of mouse calvaria with LuMa and ACE-1 cells

To evaluate the induction of new bone in the presence of LuMa cells, an in vitro bone formation model was used. Calvaria of 5- to 12-day old pups were aseptically removed and dissected from surrounding soft tissues. Two bone disks (1.5 mm) were punched and removed from the parietal bone on both sides in each calvaria using biopsy punches to create artificial defects. Calvaria were washed twice in DPBS and basal medium consisting of BGJb culture medium (Gibco, Invitrogen, Carlsbad, CA) supplemented with 0.1% bovine serum albumin (BSA) fraction V (Sigma-Aldrich Corp, St Louis, Missouri) and 100  $\mu$ g/mL Normocin (Invivogen, San Diego, CA). The calvaria with defects were divided into three groups and incubated for 12 days in BGJb culture medium  $\pm$  LuMa cells or Ace-1 cells (10 000 cells seeded on the first day) in six-well plates. BGJb medium was changed every other day in both control (BGJb + calvaria only) and treatment groups (LuMa or Ace-1 + BGJb + calvaria) until the end of the experiment. The calvarial defects were imaged at day 12 using a dissecting microscope (Nikon SMZ-U) and Nikon Diaphot 300 inverted-phase contrast microscope supplied with a Tucsen camera.

## 2.8 | Tartrate-resistant acid phosphatase and ALP staining

Calvaria were rinsed with deionized water for 10 minutes and incubated with 0.2 M citrate buffer for 5 minutes at room temperature. The calvaria were incubated with 50 mM sodium L-tartrate dehydrate (Sigma-Aldrich) in deionized water for 1 hour and transferred to acetate buffer containing 0.5 mg/mL naphthol AS-MX phosphate disodium salt (Sigma-Aldrich) and 1.1 mg/mL Fast Red TR salt 1, 5-naphthalenedisulfonate salt (Sigma-Aldrich). Calvaria were kept at 37°C for 2 hours until the red color product was developed and then rinsed using deionized water.

ALP staining of calvaria was performed using the Vector blue substrate kit (Burlingame, CA, Cat. No. SK-5300). Calvaria were

**TABLE 1** Primers used for qRT-PCR in LuMa and mouse MC3T3-E1 cells

Gene	Forward primers	Reverse primers
Canine primers		
TWIST	GGCAGGGCCGGAGACCTAGATG	TCCACGGCCTGTCTCGCTT
SNAIL	GTCTGTGGCACCTGCGGGAAG	GAAGGTTGGAGCGGTCGGCA
RUNX2	TGCCTCTGGCCTTCCACTCTCAG	TGCATTCTGGGTTGGAGAAGCG
CaR	TCTCCACGGCTGTGGCAAACC	GAGGAGTCTGCTGGAGGAGGCAT
E-cadherin	GCTGCTGACCTGCAAGGCGA	GGCCGGGTATCGGGGACAT
GAPDH	CCCCTCTTCCACCTTCGAC	AGCCAAATTCATTGTCATACCAGG
TGFβ	GGCAGAGTTGCGCCTGCTGA	CCGGTTGCTGAGGTAGCGCC
MYOF	TGCCCCGAAAGGCTGGGAAT	ACTCCGTGTGCCTGCGTCT
RANKL	TCCGAGCCGCTGTACAAAA	AGTATGAGTCTTGCCTCTCT
VIMENTIN	GAGGACATCATGCGGCTGCGG	CGCTCAAGGTCAAGACGTGCC
Osteopontin	GGTTCATATGATGGCCGAGGT	CAGAGGTGCCTCTCACTGTC
OPG	ATGCCCAGATGGGTTCTTCTC	AGAATGCCTCTCACACAAGG
CD44	CACCTCCAGTACGACACG	CATCGTCAGTGGGGTTGCT
CD133	CATTCACCGCAATTTGCCCA	ATGAGGGTCAGCAAACAGCA
Mouse primers		
OPG	AGCTGCTGAAGCTGTGGAA	TCCAGTGGCCGAGAT
UBC	CGTCGAGCCCCAGTGTACCACCAAGAAGG	CCCCCATCACACCCAAGAACAAGCACAAAG
RUNX2	CGACAGTCCCAACTTCTCTGT	TACCTCTCCGAGGGCTACAA
RANKL	GCTGGCTACCACTGGAATCT	TGTGCACACCGTATCCTTGT
Osteocalcin	CTCACAGATGCCAAGCCC	CCAAGGTAGCGCCGAGTCT
Osteopontin	GCTTGGCTTATGGACTGAGG	CGCTTTCATGTGAGAGGTG

incubated with substrate working solution for 30 minutes in the dark, washed in 200 mM Tris-HCl for 5 minutes and rinsed in deionized water. Calvaria were imaged using a dissecting microscope with camera after Tartrate-resistant acid phosphatase (TRAP) and ALP staining. Immunofluorescence of ALP in osteoblasts and newly formed bone using the Vector AP kit was detected and imaged using a Nikon Diaphot 300 fluorescent microscope.

## 2.9 | Flow cytometry

Expression of Runx2 was measured in four prostatic cancer cell lines (Ace-1, Probasco, Leo, and LuMa) using flow cytometry. The cultured PCa cells were washed twice with DPBS, trypsinized, centrifuged and counted using a Cellometer Auto T4 (Nexcelom Bioscience). One million cells were incubated with anti-Runx2 primary antibody (Cat No ab23981, 1:100 dilution; Abcam, Cambridge, MA) for 2 hours at room temperature. The cells were incubated with fluorescein goat antirabbit immunoglobulin G antibody (FI-1000, 1:100 dilution; Vector Laboratories, Burlingame, CA) for 30 minutes at 4°C, washed three times with FACS buffer (PBS, 1% BSA), and centrifuged at 1500 rpm for 5 minutes. Cells were analyzed by flow cytometry (Accuri C6; BD Biosciences, San Jose, CA). The data were analyzed with Accuri C6 Flow software (BD Biosciences).

## 2.10 | Confocal laser scanning visualization

Runx2 and ALDH1 protein expression levels were evaluated in both Ace-1 and LuMa cells using confocal microscopy. A total of 100 000 Ace-1 and LuMa cells were seeded on cover slips in 24-well plates and incubated for 24 hours at 37°C and 5% CO<sub>2</sub>. On the next day, the cells were washed twice with PBS and fixed with 4% paraformaldehyde for 30 minutes followed by PBS washing (3×) and permeabilization using methanol for 30 seconds. Ace-1 and LuMa cells were washed twice with PBS and incubated with 5% heat-inactivated goat serum for 2 hours. The cells were incubated with Runx2 (Cat No ab23981; 1:100 dilution; Abcam) or ALDH1A1 (Cat No ab23375; 1:100 dilution; Abcam) primary antibodies for 2 hours at room temperature followed by PBS washing (3×). Secondary anti-rabbit fluorescent antibody (Cat No FI-1000; 1:1000 dilution) was added to the cells for 1 hour at room temperature. The cells were washed 3× with PBS and incubated with 1 μg/mL DAPI (Cat No 62248; Life Technologies, Grand Island, NY) for 10 minutes at room temperature. Images were captured using laser scanning confocal fluorescence microscope with a 60× objective (Olympus Fluoview FV10i).

## 2.11 | ALP activity assay

The LuMa cells (before and after 5 days of incubation with calvaria) and MC3T3-E1 cells (before and after 3 days of incubation with



LuMa CM) were lysed using 1× assay buffer and Triton X-100 (0.2%), agitated for 5 minutes and centrifuged at 2500g for 10 minutes at 4°C. The standards, LuMa cells, and MC3T3-E1 cells were loaded in a 96-well plate. All samples were incubated with ALP substrate solution (p-nitrophenylphosphate [pNPP]) at room temperature for 1 hour, the stop solution was added and the absorbance was read at 405 nm (Perkin Elmer, CA). The ALP activity (u, unit) of cell lysates was measured based on the ALP standard curve.

## 2.12 | In vivo experiments

All animal experiments were approved by the Institutional Animal Care and Use Committee (IACUC) of The Ohio State University Institutional Laboratory Animal Care and Use Committee. Athymic 5-7-week-old male nude mice (NCr-nu/nu) were purchased from the OSU Comprehensive Cancer Center (OSUCCC) Target Validation Shared Resource (TVSR). Mice were maintained according to the NIH standards established in the “Guidelines for the Care and Use of Laboratory Animals.”

### 2.12.1 | Subcutaneous, intratibial, and intracardiac injection of LuMa cells into nude mice

#### *Subcutaneous*

Two million luciferase/YFP-transduced LuMa cells (LuMa-Luc) suspended in 0.25 mL of sterile DPBS were injected subcutaneously in four mice above the right shoulder using a 25-gauge needle. Tumor volume was measured twice weekly using a digital caliper. Three dimensions were measured, and tumor volume was calculated using the formula; length × width × height × 1/2. Tumor growth rate in SQ xenografts was measured weekly using bioluminescent imaging. The doubling time for the tumor volume was calculated using the formula; doubling time = duration (days) × log (2)/log (final volume/initial volume).

#### *Intratibial*

Nude mice (N = 5) were maintained under isoflurane anesthesia (2.5%) in supine position during intratibial (IT) injection. The right leg was held and the knee joint was bent so the femur made a 90° angle with the tibia. LuMa-Luc cells (50 000 in 10 µL) were loaded in a Hamilton syringe with 27-gauge needle. The needle was placed through the patellar ligament and the articular cartilage of the tibia into the metaphyseal marrow space of the tibia. IT tumor growth was monitored weekly by bioluminescent imaging.<sup>33</sup>

#### *Intracardiac*

Nude mice (N = 6) were anaesthetized using 3% isoflurane initially and 2.5% during the intracardiac (IC) procedure. The mice were placed on their back and their front and hind legs were restrained to the procedure table with surgical tape. A tuberculin syringe with 0.1 mL of DPBS containing 100 000 LuMa-Luc cells and 0.1 mL of air was prepared. The syringe with a 27-gauge needle was introduced into the left ventricle of the heart through the third intercostal space

(1 mm to the left and lateral from the sternum). Once a jet of blood was present in the hub of the needle, the cell suspension was then slowly injected for 30 seconds.<sup>33</sup> Bioluminescent imaging was performed directly postinjection (7-10 minutes) to ensure successful IC injection and weekly to monitor for metastases.

## 2.13 | Bioluminescent imaging

D-Luciferin (0.1 mL of 40 mg/mL, dissolved in DBPS) was injected intraperitoneally in each mouse before anesthesia using a 1 mL tuberculin syringe (Caliper Life Sciences). Mice were anesthetized with 3% isoflurane and maintained with 2% isoflurane during bioluminescent imaging. The IVIS 100 (Caliper Life Sciences, Hopkinton, MA) was used to detect the bioluminescence and the photon signal intensity (total photons/sec) was measured for each region of interest using Living Image software version 2.50 (Caliper Life Sciences). Imaging was performed every 1 minute until the peak signal was obtained (10-15 minutes postinjection). The IVIS 100 was set to a 1-minute exposure with medium binning.

## 2.14 | Radiography

Radiography was performed on the right hind leg in IT and both the right and left hind legs for IC experiments. Formalin-fixed legs were soaked in water for 8 hours and then placed centrally on a Faxitron laboratory radiography system LX-60 (Faxitron X-ray Corp, Wheeling, IL) imaging platform and high resolution DICOM radiograph images were taken at 25 KeV with 5-second exposures.

## 2.15 | Histopathology

The animals were euthanized after 21 days in the IC experiment and 30 days in both the SQ and IT experiments. Tumors, tissue specimens and bones were collected at necropsy. Tumor and tissue specimens were fixed in 10% neutral-buffered formalin at room temperature for 72 hours, embedded in paraffin, cut in 4 µm sections, and stained with hematoxylin and eosin (H&E). Bones were decalcified with mild Decalcifier (formaldehyde, methanol and formic acid; Leica Biosystems, Buffalo Grove, IL) at room temperature for 6 hours. Histological images of the slides were taken using an Olympus BX51 microscope equipped with a Nikon digital camera and analyzed using ImageScope software (version 11.2; Leica Biosystems, Buffalo Grove, IL).

## 2.16 | Immunohistochemistry

Paraffin-embedded tissue sections (4-µm thick) were preheated at 60°C for 1 hour, dewaxed, rehydrated and incubated with antigen

retrieval solution (Dako, Carpinteria, CA) for 50 minutes in a steamer (Black & Decker HS1000, Newark, DE) followed by slow cooling. To eliminate endogenous peroxidase activity, slides were treated with 3% hydrogen peroxide (H<sub>2</sub>O<sub>2</sub>), washed, and coated with serum free protein block (Dako). Tissue sections were incubated with primary antibodies to RUNX2, E-cadherin, cytokeratin AE1/AE3, PTHrP, and Twist overnight at 4°C (Table 2). Secondary biotinylated antibodies were applied on the second day for 30 minutes, followed by incubation with diaminobenzidine (DAB; Dako) for 5 minutes and counterstained with hematoxylin. Sections were dehydrated through graded alcohols and xylene and coverslipped. DAB brown color staining was recorded as a positive reaction. Positivity and intensity of staining was evaluated as weak, moderate, or strong using Aperio digital scans, ImageScope software (version 11.2; Leica Biosystems) and the algorithm positive pixel count analysis (version 9).

### 2.17 | Statistical analysis

All data were displayed as mean ± standard deviation. One-way analysis of variance was used to analyze normalized gene expression data and tumor volume and bioluminescence in mice followed by Sidak's multiple comparisons test using GraphPad Prism version 6.03 (La Jolla, CA). Data with  $P \leq .05$  were considered statistically significant.

## 3 | RESULTS

### 3.1 | Histopathology of the primary carcinoma and subcutaneous xenograft

The primary prostate carcinoma had a papillary to cribriform pattern (Figure 1A,B). Foci of transitional cell differentiation with vacuolated cells were present. Desmoplasia was pronounced throughout the tumor parenchyma with multifocal areas of necrosis and squamous metaplasia. Chronic submucosal edema and urothelial hyperplasia were reported in the bladder with mild mesothelial hypertrophy and hyperplasia. No neoplastic changes were observed in the bladder epithelium. Multifocal metastatic well-differentiated carcinomas with central necrosis and mineralization were present in the lungs of the dog.

LuMa subcutaneous (SQ) xenografts were grossly visible in nude mice 1 week after implantation. Mice were euthanized 1 month after

tumor implantation, and the average tumor volume was  $2.1 \pm 1.2 \text{ cm}^3$ . SQ xenografts were easily dissectible from the SQ tissue. The histological characteristics of the SQ tumors were similar to the primary prostatic carcinoma and contained foci of necrosis (Figure 1C,D).

### 3.2 | In vitro and in vivo growth and culture characteristics

The LuMa cells formed a cobblestone growth pattern in culture. The average diameter of LuMa cells in cell culture was 13.5 to 15.3 microns. LuMa cells grew in a monolayer sheet consisting of polygonal cells and few moderate to large oval cells (22–28 microns) with a large vesicular nucleus and prominent nucleoli (Figure 2A). The doubling time of LuMa cells in culture was  $30.8 \pm 1.4$  hours in standard culture conditions (Figure 2B). In vivo, the doubling time of the tumor volume in LuMa SQ xenografts was approximately  $8.6 \pm 2.6$  days (Figure 2C).

### 3.3 | STR DNA profiling and multiplex PCR analysis of LuMa cells

LuMa cell line was confirmed to be of canine origin with no mammalian interspecies contamination. A genetic profile for LuMa was generated using a panel of 14 STR markers for genotyping compared to Ace-1 cells (Supporting Information Table S).

### 3.4 | Immunohistochemistry, confocal microscopy, and flow cytometry

Immunohistochemistry revealed strong staining of Runx2 in the cytoplasm of LuMa cells in both SQ and bone xenografts (Figure 3A,B). Primary LuMa tumors were strongly positive for epithelial markers (cytokeratin AE1/AE3 and E-cadherin; Figure 3C,D). LuMa primary cancer cells had intense cytoplasmic and nuclear staining for PTHrP and moderate cytoplasmic staining for Twist (Figure 3E,F).

Flow cytometric analysis revealed that few Ace-1, Probasco, and Leo cells were positive for Runx2 ( $0.2 \pm 0.05\%$ ,  $0.16 \pm 0.05\%$ , and  $2.8 \pm 1.5\%$ , respectively; Figure 4A–C) while many LuMa cells expressed Runx2 ( $12.4 \pm 0.43\%$ ; Figure 4D). LuMa and Leo cells

**TABLE 2** Antibodies used for immunohistochemistry of LuMa primary tumor and mouse xenografts

Antibody	Species	Clone	Company	Dilution
CK AE1/AE3	Mouse	M3515	Dako Corporation, Carpinteria, CA	1:100
Twist	Rabbit	H81	Santa Cruz Biotechnology, Santa Cruz, CA	1:150
PTHrP	Goat	N-19	Santa Cruz Biotechnology, Santa Cruz, CA	1:200
Runx2	Rabbit	ab23981	Abcam, Cambridge, MA	1:100
E-cadherin	Mouse	Clone 36	BD Biosciences, San Jose, CA	1:200

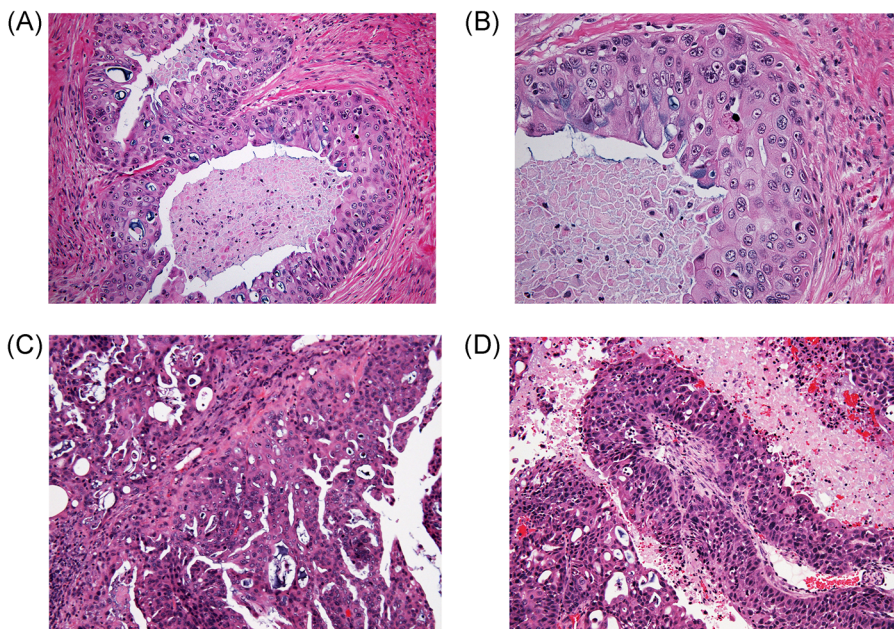


**FIGURE 1** Histopathology of LuMa primary prostatic carcinoma (A,B) and the subcutaneous xenografts (C,D) in nude mice (H&E stain). LuMa neoplastic cells in the primary tumor had a cribriform pattern (A,B) (200 $\times$  and 400 $\times$ , respectively). (C,D) LuMa cells in SQ xenograft tumors had a cribriform to papillary pattern with transitional cell-like differentiation (200 $\times$ ) [Color figure can be viewed at [wileyonlinelibrary.com](http://wileyonlinelibrary.com)]

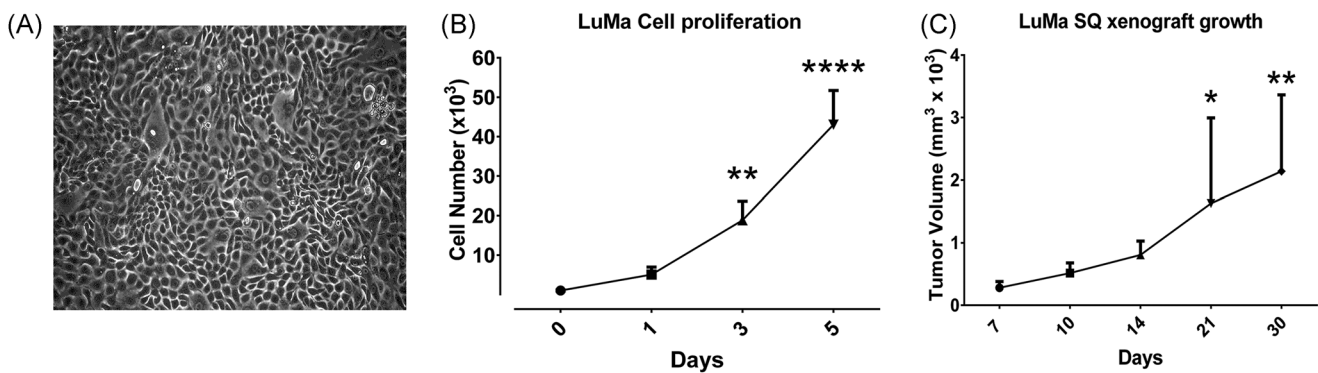


**FIGURE 2** In vitro and in vivo growth characteristics of LuMa cells. A, Phase contrast microscopy of LuMa cells in culture with a cobblestone pattern. B, In vitro growth curve of LuMa cells in vitro. Data are mean  $\pm$  SD of three replicates for each time point. C, Graph shows mean LuMa tumor volume in SQ xenografts. Data presented as a mean  $\pm$  standard deviation from five mice

had greater Runx2 (46  $\pm$  1.6-fold and 11  $\pm$  0.9-fold, respectively) compared to the Ace-1 cells.

The differences between Ace-1 and LuMa cells in Runx2 and ALDH1A expression and cellular distribution were also examined by confocal microscopy. Both Ace-1 and LuMa cells were positively stained with Runx2 and ALDH1A antibodies. Runx2 staining was strong and diffuse in the cytoplasm of LuMa cells compared to Ace-1 cells which had weak cytoplasmic staining (Figure 4E,F). Intense ALDH1A staining was observed mainly around the nuclei of LuMa cells compared with Ace-1 cells (Figure 4G,H).

### 3.5 | qRT-PCR of LuMa cells in vitro

LuMa cells had significantly greater mRNA expression for *RUNX2* ( $P = .037$ ), *MYOF* ( $P = .029$ ), *CD44* ( $P = .0002$ ), *OPN* ( $P = .0001$ ) and

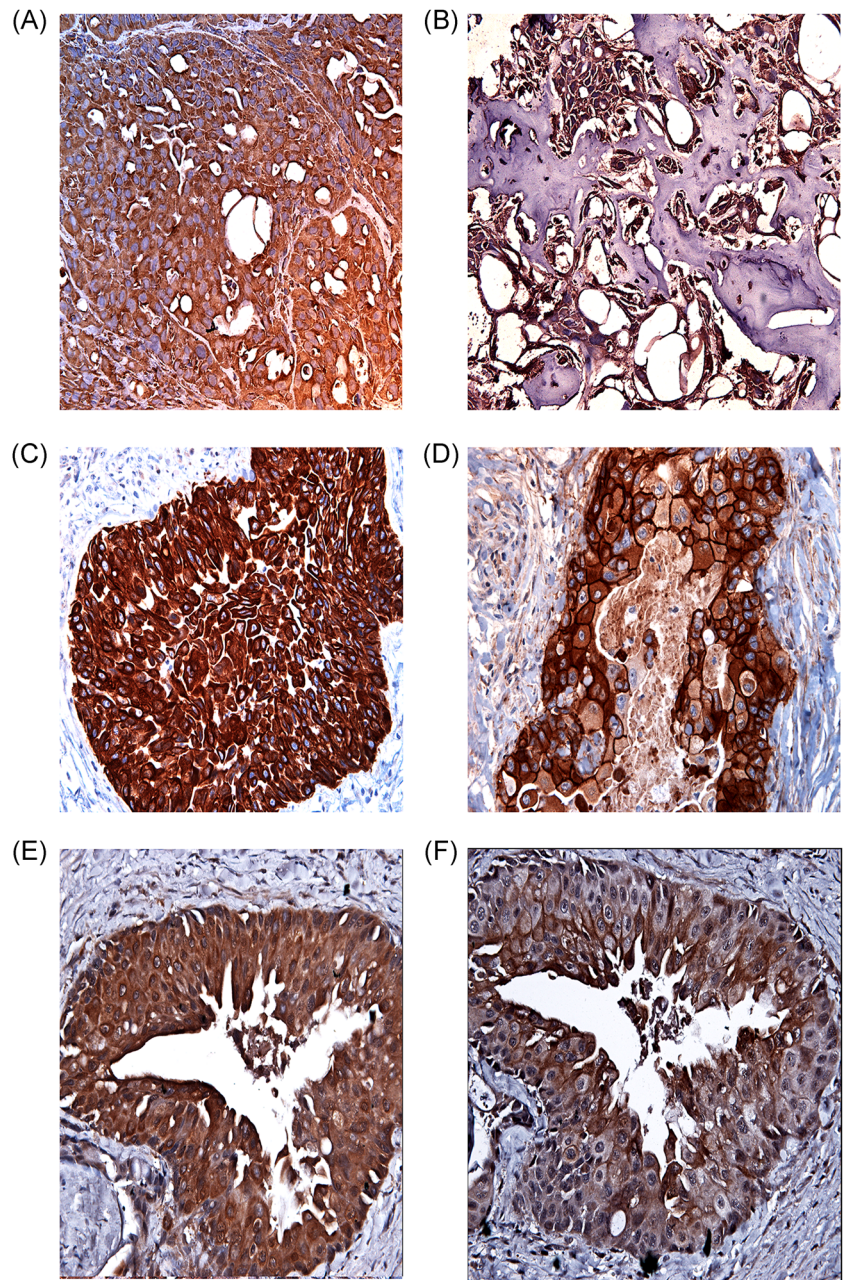
*CDH1* (*E-cadherin*) ( $P = .049$ ) compared to normal prostate tissue, BPH, and canine prostatic cancer cell lines (Ace-1, Probasco, and Leo) (Figure 5A,B). There was little to moderate mRNA expression of mesenchymal markers (*VIMENTIN* and *SNAIL*) in LuMa cells compared to Ace-1 cells (Figure 5C). There was weak to no expression of *AR*, *TWIST*, *CDH2* (*N-cadherin*), *GRPR*, and *IGF-1* mRNA in LuMa cells (data not shown). LuMa cells expressed significantly less *FOLH1* mRNA than Leo ( $P = .0044$ ) and Probasco ( $P = .0429$ ) cells and a similar level of *CD133* mRNA compared to Probasco cells (Figure 5D).

### 3.6 | Effect of LuMa on bone formation in mouse calvaria defects

LuMa cells improved the healing response of calvarial defects when compared to Ace-1 and control calvaria. The calvarial defects in the



**FIGURE 3** IHC staining of Runx2 in LuMa subcutaneous (A) and intratibial (B) xenograft tumors (200×). IHC staining of cytokeratin AE1/AE3 (C) (200×), E-cadherin (D) (400×), PTHrP (E) (200×) and Twist (F) (200×) in LuMa primary prostatic carcinoma. LuMa cells were strongly positive for Runx2, cytokeratin, E-cadherin, PTHrP and moderately positive for Twist. Many LuMa cells had nuclear staining for PTHrP. IHC, immunohistochemistry [Color figure can be viewed at [wileyonlinelibrary.com](http://wileyonlinelibrary.com)]



control group (without any cancer cells) had no stromal cell growth and an eroded border with no evidence of osteoblast cell proliferation (Figure 6A,B). Calvaria incubated with Ace-1 cells had mild to moderate stromal growth in the defects with eroded margins (Figure 6C,D). The calvarial bone defects developed growth of osteoblasts and stromal cells into the defects with bone mineralization in culture with LuMa cells (Figure 6E-H).

ALP and TRAP staining were performed to identify osteoblasts and osteoclasts in the reparative tissue. The majority of the cells were ALP-positive blue (using an inverted microscope) or green (using a fluorescent microscope) and were interpreted as osteoblasts (Figure 6I-K). There were few TRAP-positive osteoclasts at the border of the defects (data not shown).

### 3.7 | Effect of LuMa on MC3T3-E1 osteoblast differentiation

There were morphological differences in MC3T3-E1 cells after incubation with LuMa CM. MC3T3-E1 cells formed a monolayer of ovoid to pyriform cells with clear cytoplasm (Figure 7A). After incubation with LuMa CM, MC3T3-E1 cells had many small vacuoles in the cytoplasm close to the cell border (Figure 7B). To determine whether LuMa CM induced MC3T3-E1 cell differentiation, ALP activity and the expression of osteogenic-related genes mRNA were measured in MC3T3-E1 cells. Cotreatment of MC3T3-E1 cells with LuMa CM increased ALP activity in the MC3T3-E1 cells compared to untreated cells ( $P = .011$ ) (Figure 7C). In addition,

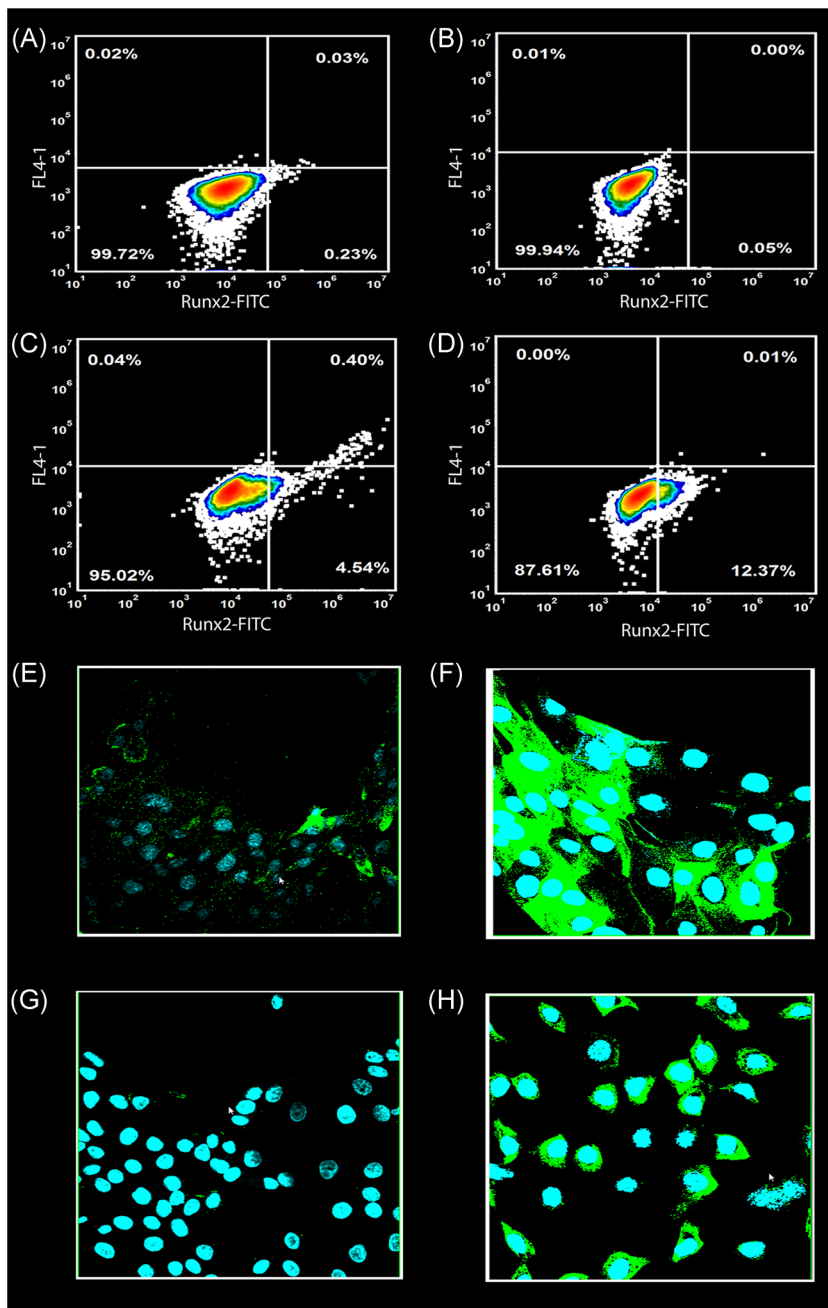


**FIGURE 4** Flow cytometric and confocal microscopic analysis of Runx2 and ALDH1 in canine prostate cancer cell lines. A-D, Flow cytometric analysis of Ace-1 (A), Probasco (B), Leo (C), and LuMa (D). The number in the lower right corner indicates the percentage of Runx2-positive cells in each cell line. E-H, Confocal microscopic images of Runx2 (E-F) and ALDH1 (G-H) expression level in Ace-1 (E, G) and LuMa (F, H) cell lines [Color figure can be viewed at [wileyonlinelibrary.com](http://wileyonlinelibrary.com)]

LuMa CM upregulated the mRNA expression level of *RUNX2* (2.0-fold) ( $P = .0017$ ) in MC3T3 E1 cells compared to untreated cells (Figure 7D). There was a significant increase in *OPG* mRNA (2.3-fold) ( $P = .00019$ ) in the treated MC3T3-E1 cells and no change in *RANKL* mRNA ( $P = .85$ ) (Figure 7D). This resulted in an increased the *OPG/RANKL* ratio in LuMa CM-treated MC3T3-E1 cells ( $P = .0134$ ).

### 3.8 | Effect of bone (calvaria) and bone CM on LuMa ALP activity and gene expression

LuMa cells had greater ALP activity ( $P = .0059$ ) compared to Ace-1 cells. However, there was a marked decrease in ALP in LuMa cells

( $P = .0062$ ) after incubation with calvaria for 5 days (Figure 7E). Calvaria increased the expression of *CaR* (5.6-fold) ( $P = .00028$ ) and *TGF $\beta$*  (1.7-fold) ( $P = .024$ ) mRNA in LuMa cells. In addition, there was a trend for *RUNX2* expression to be increased (Figure 7F). Calvaria downregulated the mRNA expression of *OPG* (0.4-fold) ( $P = .0001$ ) and *OPN* (0.14-fold) ( $P = .0046$ ) in LuMa cells (Figure 7F).

### 3.9 | IT injection of LuMa cells in nude mice

The tibias of nude mice with LuMa tumors had radio-opaque areas in the epiphysis, metaphysis, and diaphysis of the marrow cavity (Figure 8A). Histopathological examination of the tibias showed



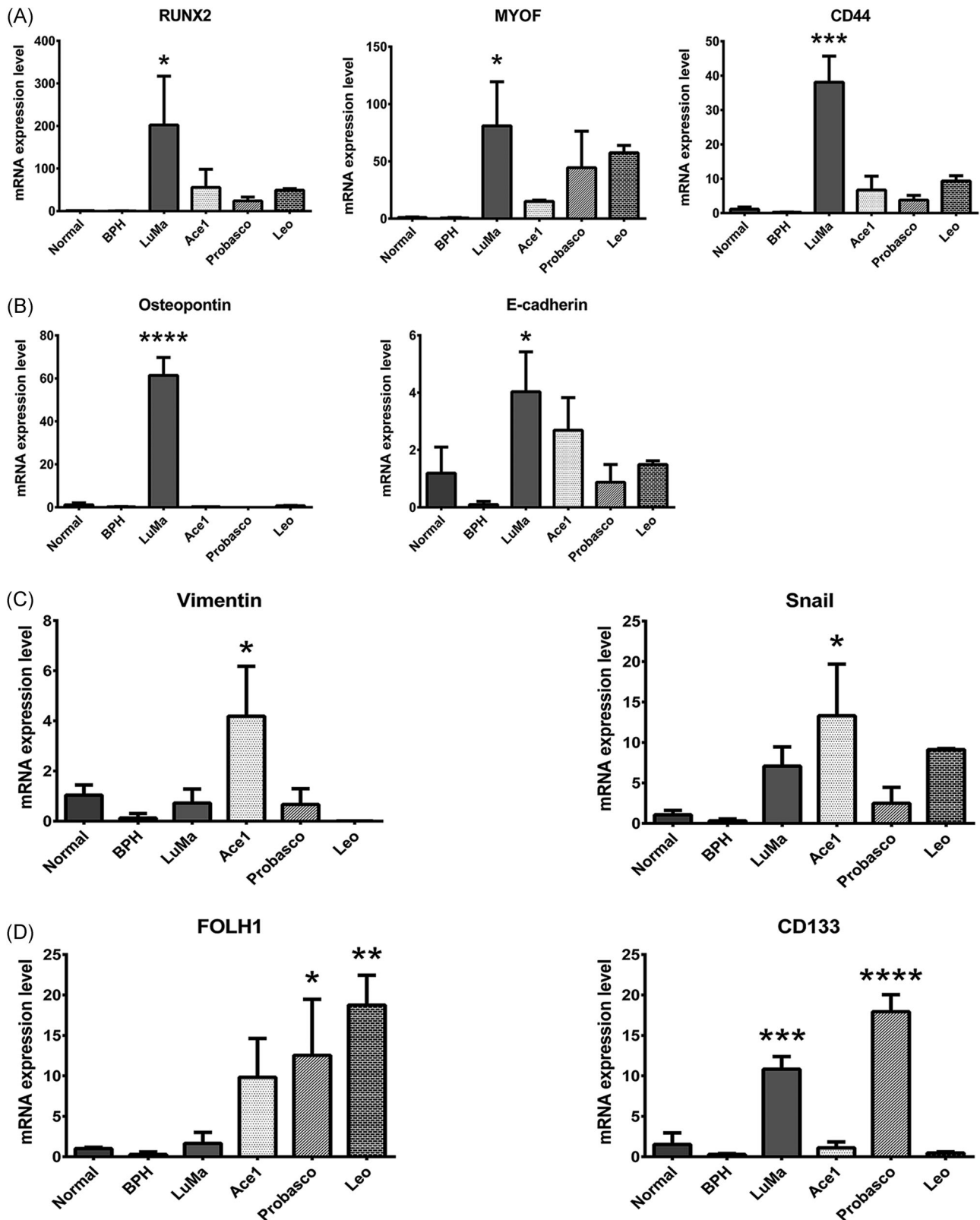


**FIGURE 5** A-B, The mRNA expression of RUNX2, MYOF, CD44, Osteopontin, and E-cadherin in normal dog prostate ( $n = 2$ ), BPH ( $n = 2$ ) and prostate cancer cell lines (Ace-1, Probasco, Leo, and LuMa). C-D, The expression of mesenchymal markers (VIMENTIN and SNAIL), FOLH1 (PSMA) and CD133 (PROMININ) in normal prostate ( $n = 2$ ) and BPH ( $n = 2$ ) tissues, and four canine prostatic cancer cell lines. The graphs represent the relative mRNA expression in Ace-1, Probasco, Leo, and LuMa cells in comparison to normal prostate gland. Significant differences are indicated as  $*P \leq .05$ ,  $**P \leq .01$ ,  $***P \leq .001$ , and  $****P \leq .0001$  different from normal prostate. BPH, benign prostatic hyperplasia

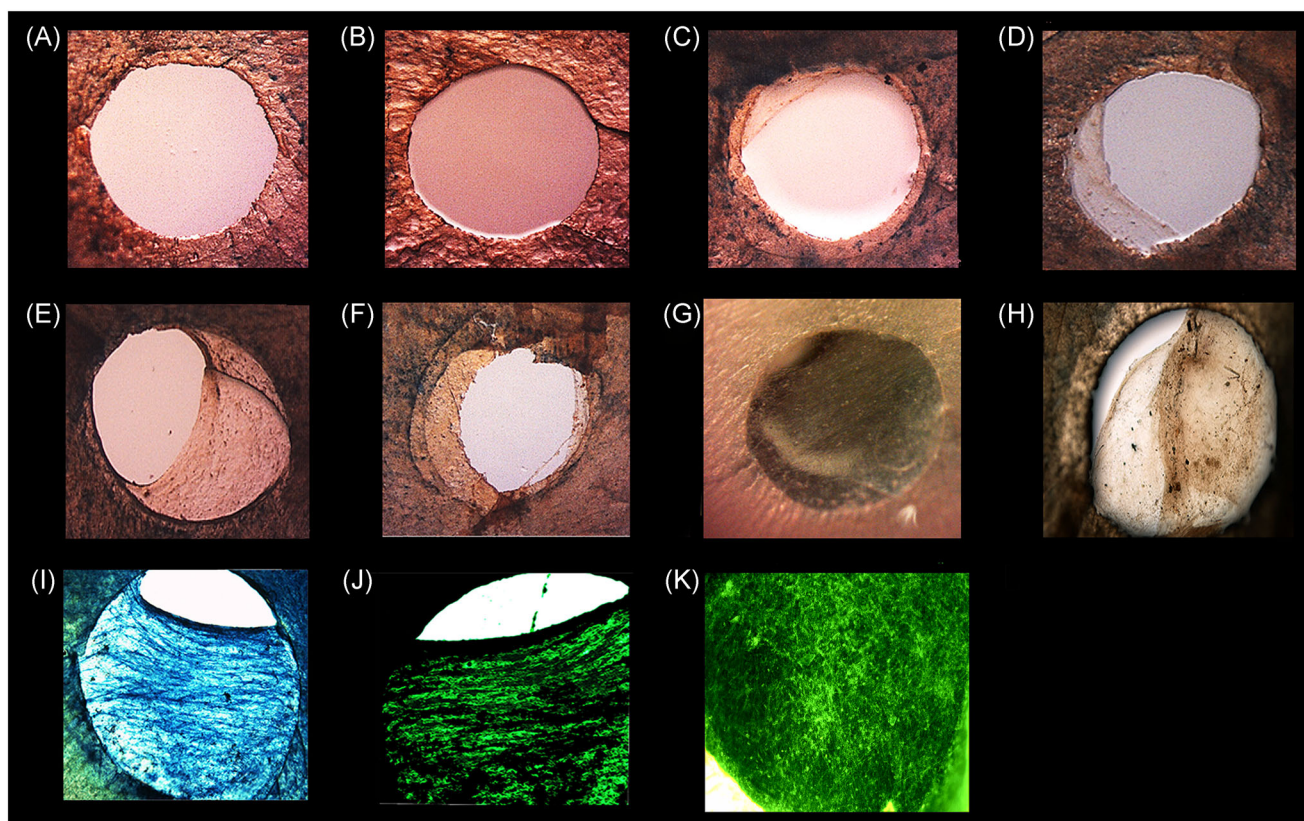


**FIGURE 6** Effect of LuMa cells on mouse calvarial defects. Dissecting (A-H), phase contrast (I) and fluorescent (J, K) microscopic images showing the effect of LuMa cells on growth and mineralization of calvarial defects in vitro. A-B, The calvarial defect incubated with only BGJb showed regular and irregular perimeters. C-D, The calvarial defect incubated with Ace-1 cells was partially (15-20%) filled by osteoblasts and mineralized matrix with irregular perimeters. E-H, The defect was partially to almost closed with osteoblast and stromal cells in calvaria incubated with LuMa cells. I-K, The defects were almost completely closed by osteoblast and stromal cells in LuMa-incubated calvaria; the osteoblasts stained positive for alkaline phosphatase (blue, light microscopy) (I) or (green, fluorescent microscopy) (J-K) [Color figure can be viewed at [wileyonlinelibrary.com](http://wileyonlinelibrary.com)]

compact sheets of neoplastic LuMa cells and large multifocal areas of new intramedullary woven bone lined by hypertrophic cuboidal osteoblasts adjacent to neoplastic cells. LuMa cells induced new bone formation from the endosteal and trabecular surfaces (Figure 8B-D).

### 3.10 | IC injections and bioluminescent imaging of LuMa in nude mice

The metastasis of LuMa cells after left ventricular intracardiac injection was monitored by bioluminescence imaging. Successful IC injections were confirmed using bioluminescence at 7 minutes, which demonstrated distribution of tumor cells throughout the body (Figure 9A). The bioluminescence diminished after 1 to 2 days and was negative until day 18. At 3 weeks, four of six nude mice had bioluminescence in their long bones (tibia, humerus, and femur), head, vertebrae, and adrenal glands (Figure 9A). Radiographic images demonstrated mild medullary sclerosis in the metaphysis of long bones (tibia and humerus) (Figure 9B). The locations of LuMa metastases (confirmed by microscopic examination) were reported (Table 3). Histological examination showed that LuMa metastases in the tibias, humeri, and femurs were characterized by mild to

moderate osteoblast cell proliferation, new bone formation, and displacement of bone marrow cells (Figure 9C,D). LuMa metastatic tumors occupied most of the vertebral medullary bone and surrounded by hypertrophic and hyperplastic osteoblasts (Figure 9E). LuMa metastases were also in the adrenal glands, brain, and mandibular alveolar bone (Figure 9F-H).

## 4 | DISCUSSION

Canine prostate cancer is considered an excellent model of human PCa for several reasons. Prostate carcinoma occurs spontaneously in older dogs, is usually androgen-independent, and commonly metastasizes to bone, lung, and regional lymph nodes.<sup>35</sup> Several canine PCa cell lines have been developed that recapitulate the late stages of prostate cancer progression and bone metastasis and are useful to investigate the interaction that occurs between PCa cells and bone microenvironment.<sup>36,37</sup> Few human PCa tumor and cell lines can be used to model osteoblastic bone metastasis, these include LuCaP 23.1, LAPC-9, VCaP, and LNCaP C4-2B.<sup>29,34,38,39</sup> MDA-PCa 2b is a human prostatic cell line that forms osteoblastic bone metastasis after about 2 to 3 months of intraosseous injection.<sup>32</sup> In this study,

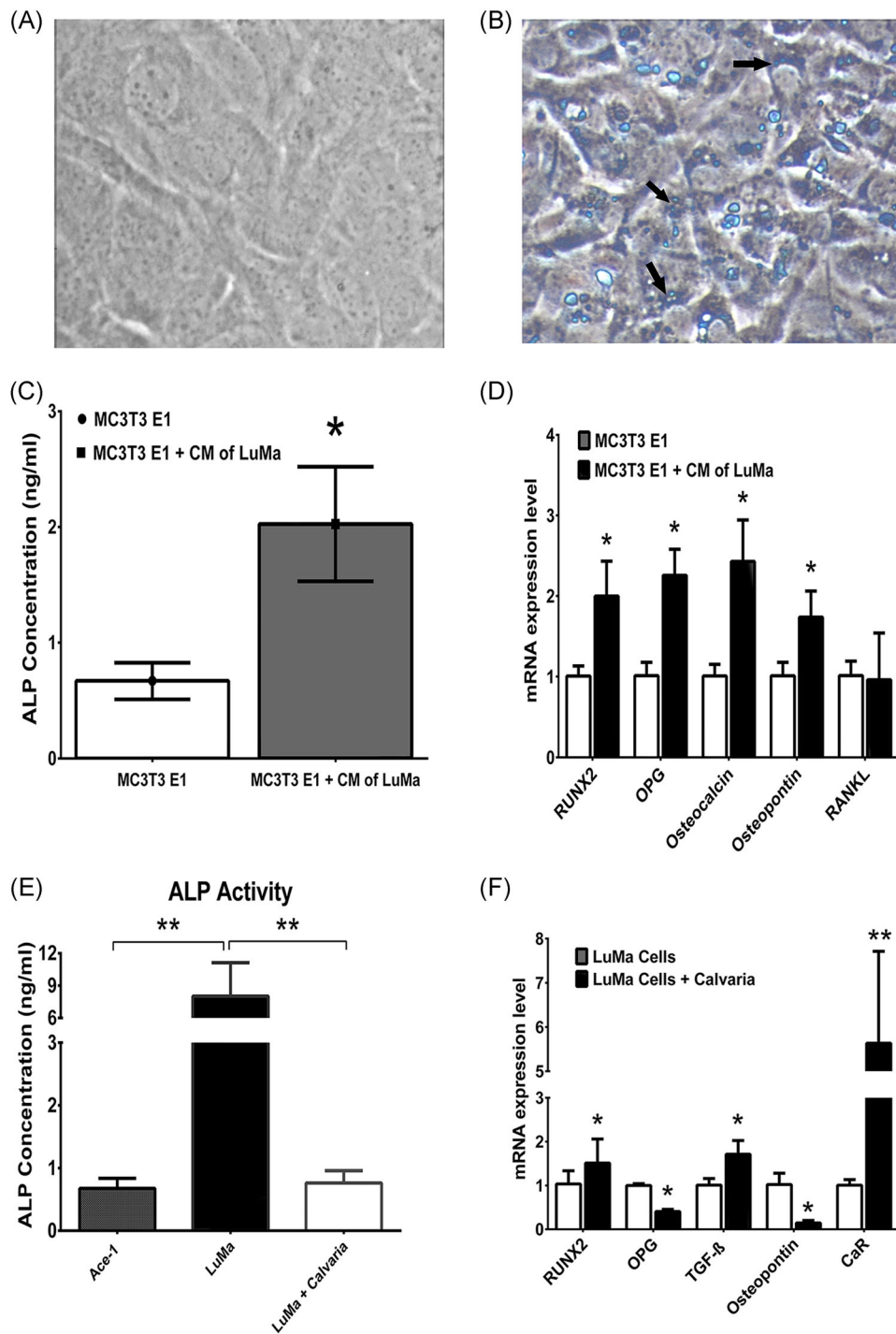


**FIGURE 7** A-B, Effect of LuMa CM on MC3T3-E1 cells. Phase-contrast photomicrographs of control (untreated) (A) and LuMa CM-treated (B) MC3T3-E1 cells. B, MC3T3-E1 cells had cytoplasmic vacuoles (arrows) after LuMa CM treatment. C-D, Effect of LuMa CM on MC3T3-E1 cells, alkaline phosphatase activity and gene expression. C, Concentration of alkaline phosphatase in control MC3T3-E1 cells and cells treated with LuMa CM. D, qRT-PCR of mRNA expression of bone-related genes (RUNX2, OPG, Osteocalcin, Osteopontin, and RANKL) in MC3T3-E1 cells with and without treatment with LuMa CM. E-F, Effect of bone (calvaria) on LuMa ALP activity and gene expression. E, Concentration of alkaline phosphatase in Ace-1 and LuMa cells (before and after incubation with calvaria). F, qRT-PCR of expression of RUNX2, OPG, TGFβ, Osteopontin and CaR mRNA in LuMa cells ± calvaria. Significant differences are indicated as \* $P \leq .05$ , \*\* $P \leq .01$ , \*\*\* $P \leq .001$ , and \*\*\*\* $P \leq .0001$ . CM, condition media; OPG, osteoprotegrin; qRT-PCR, quantitative reverse-transcription polymerase chain reaction; TGFβ, transforming growth factor β [Color figure can be viewed at [wileyonlinelibrary.com](http://wileyonlinelibrary.com)]



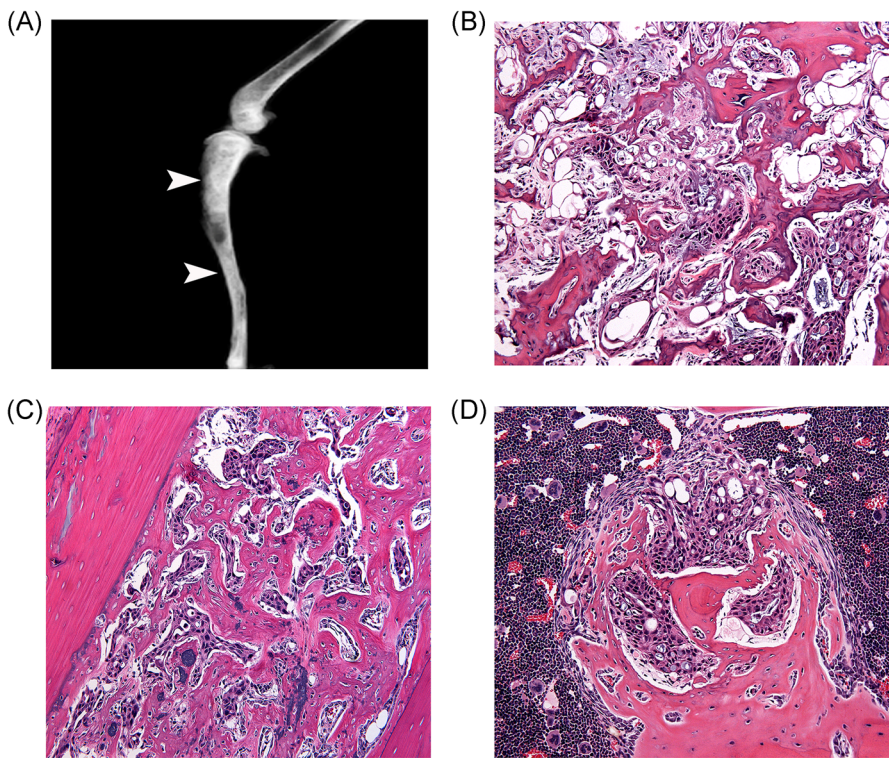


**FIGURE 8** LuMa xenografts in the tibia of nude mice. A, Radiography of intratibial LuMa tumors with radiopaque intramedullary osteoblastic tumors (arrows). Histopathology of LuMa tibial tumor (B-D) showing intramedullary new bone formation emanating from endosteal and trabecular bone lined with hypertrophic osteoblasts (200 $\times$ ) [Color figure can be viewed at [wileyonlinelibrary.com](http://wileyonlinelibrary.com)]

we showed that LuMa cells formed osteoblastic bone metastasis after IT or IC injection.

Seven canine prostate cancer cell lines (Ace-1, Probasco, Leo, DPC-1, CPA-1, CHP-1, and CT-1258) have been described. The Ace-1 cell line has been used extensively in prostatic cancer research. Ace-1 cells have been easily transfected with human or dog genes such as *PTHrP*, *GRPr*, and *DKK1* for studying different signaling pathways in prostate cancer. Orthotopic injection of Ace-1 cells in dogs resulted in prostatic tumors with metastases to lungs and lymph nodes.<sup>39</sup> Ace-1 cells grow in vitro, metastasize to long bones after intracardiac injection and induced mixed osteoblastic/osteolytic metastases after intraosseous injection in nude mice.<sup>27</sup> The Leo cell line has been useful to investigate brain metastasis and osteolytic bone metastases in prostate cancer.<sup>34</sup> The LuMa and Probasco<sup>33</sup> cell lines induce prominent osteoblastic bone metastases in nude mice following IT injection. Probasco induces new woven bone that emanates from the periosteal surface in the form of a radio-opaque starburst pattern radiographically and histologically, while the endosteal new bone was characterized by sclerosis of bone marrow cavity with loss of bone trabeculae.<sup>33</sup> In contrast, LuMa cells mainly induced new woven bone formation from the endosteum and within the marrow cavity with disruption of the trabeculae. CHP-1 is a useful cell line to study androgen receptor (AR) signaling in both AR-dependent and -independent PCa.<sup>40</sup> CHP-1 cells have not been extensively characterized in terms of their metastasis sites and bone metastasis phenotype. The DPC-1 cell line has been utilized for imaging of PCa in both mice and dogs by targeting PSMA. DPC-1 cells are highly tumorigenic in nude mice and orthotopically in immunodeficient

dogs.<sup>41,42</sup> DPC-1 cells showed metastatic potential in vivo indicated by the presence of lung and iliac lymph node micrometastases in immunosuppressed dogs after orthotopic injection. DPC-1 cells induced mixed osteoblastic and osteolytic bone metastases similar to Ace-1 cells.<sup>42</sup> The CPA-1 cell line produces well-differentiated prostatic tumors with acinar pattern in athymic mice similar to the primary tumor with no evidence of metastasis.<sup>43</sup> It has been demonstrated that CT-1258 cell line is tumorigenic in NOD-SCID mice following SQ or intraperitoneal implantation without any further metastases.<sup>44</sup>

LuMa cells had increased osteomimicry properties compared to Probasco, Ace-1, and Leo cells as evidenced by the expression of bone-associated markers (*RUNX2*, *ALP*, and *OPN*) and by their ability to induce calcified bone matrix in a calvarial defect in vitro compared to Ace-1 cells. Upregulation of *Runx2* expression in carcinomas was found to be correlated with enhanced tumor progression, skeletal metastasis<sup>45,46</sup> and a poor prognosis.<sup>26</sup> Some previous studies demonstrated that knockin of *RUNX2* was accompanied with an increase in the expression of osteogenic genes including *OPN*, *OC*, *RANKL*, and *MMP-9*, which promoted skeletal metastases of solid tumors.<sup>47-51</sup> Some functional studies have shown that overexpression of *OPN* in PCa cell lines increased cancer cell invasion and enhanced their ability to enter the circulation in mouse models.<sup>52</sup> Based on these data, we propose that *Runx2* and *OPN* signaling plays an important role in osteomimicry, tumorigenesis, and bone metastasis of LuMa cells.

LuMa cells induced the differentiation of murine MC3T3-E1 cells to express osteoblast genes (*OPN* and *OC*) and proteins (*ALP*). *ALP* activity,

**FIGURE 9** Bioluminescence and histopathology of LuMa IC xenografts. A, Bioluminescent images of nude mice after 7 minutes (1), 15 minutes (2), 18 days (3) and 21 days (4, 5). B, Radiographic image of intratibial LuMa tumors 21 days after intracardiac injection showing a radiopaque area in epiphysis and metaphysis of the tibia (arrowhead). C–H, Histopathological images showing LuMa metastases (arrowheads) in the tibia (C) (100 $\times$ ), humerus with inset (D) (100 $\times$ ), cervical vertebra (E) (200 $\times$ ), adrenal gland (F) (200 $\times$ ), brain (G) (400 $\times$ ) and alveolar bone of a tooth (H) (200 $\times$ ) [Color figure can be viewed at [wileyonlinelibrary.com](http://wileyonlinelibrary.com)]

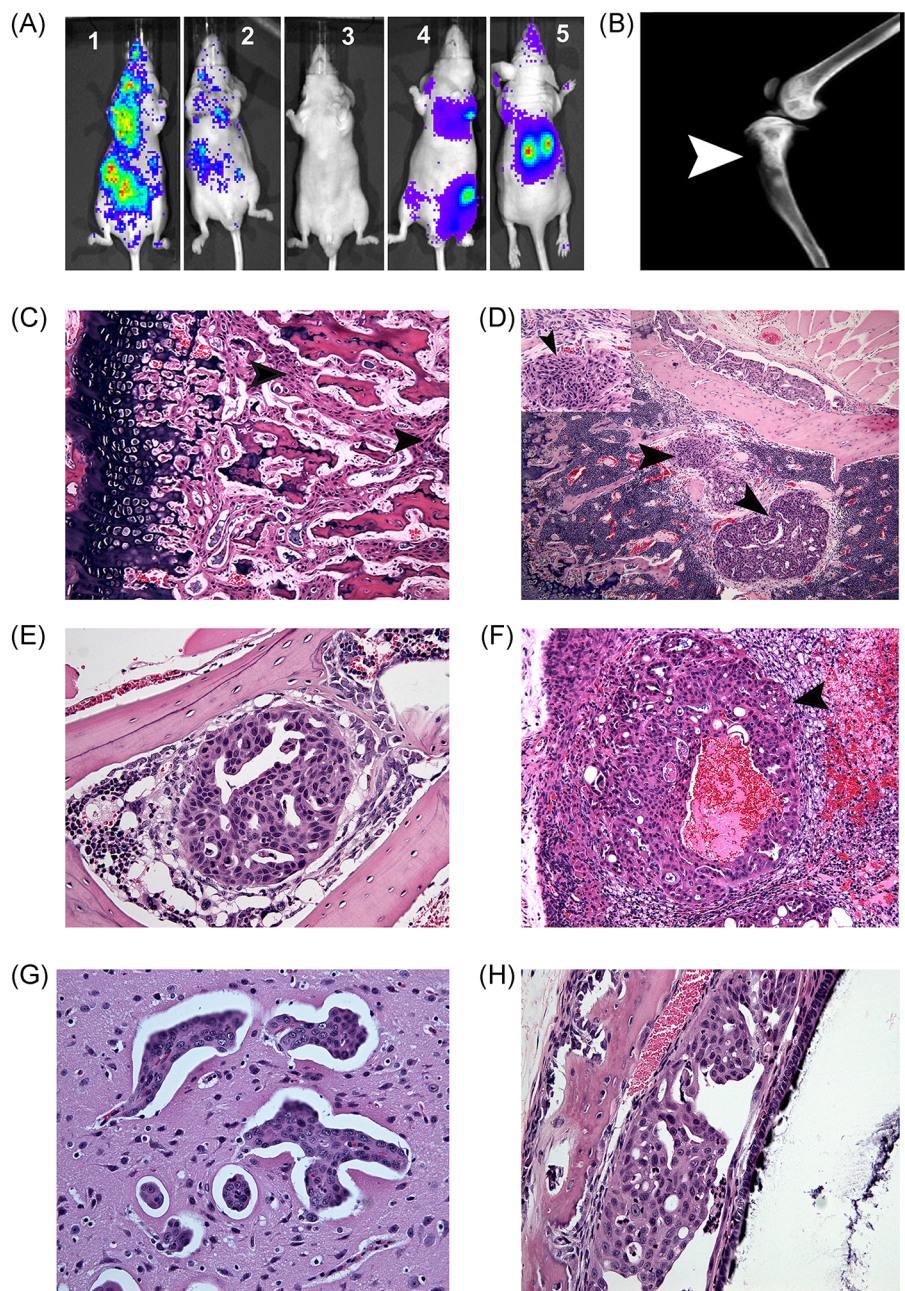


**TABLE 3** LuMa metastases in nude mice at 21 d following left ventricular injection

Mouse #	Metastasis sites
Mouse 1	Tibia, femur, vertebrae and adrenal gland
Mouse 2	Tibia, mandible and brain (undetected by bioluminescence)
Mouse 3	Tibia, femur, vertebrae, brain and adrenal gland
Mouse 4	Null
Mouse 5	Tibia, femur, vertebrae, brain and adrenal gland
Mouse 6	Tibia, femur, vertebrae, mandible and adrenal gland

production of bone sialoprotein, OC, and mineralization are parameters that are typically used to identify osteoblastic differentiation.<sup>53</sup>

LuMa cells may have inhibited osteoclastic bone resorption in the osteosclerotic bone metastases by increasing the production of OPG and decreasing RANKL. In vitro, LuMa cells increased the OPG/RANKL ratio in MC3T3-E1 cells suggesting that LuMa decreased osteoclastogenesis by its regulation of OPG/RANKL gene expression with subsequent disruption of RANK/RANKL signaling in osteoclasts. The RANK/RANKL/OPG triad is the master regulator of osteoclast function in vivo. Binding of RANKL produced from osteoblasts to its receptors (RANK) on osteoclasts promotes osteoclast differentiation and its resorptive activity.<sup>54–57</sup> OPG is a decoy



receptor for RANKL and inhibits the ability of RANKL to induce osteoclast function.<sup>55,58</sup>

LuMa cells will also be useful to investigate cancer stem cell (CSC) markers in prostate cancer. They expressed high levels of ALDH1 protein and CD133 and CD44 mRNA. It has been shown that CD44,  $\alpha 2\beta 1$  and CD133-expressing PCa cells exhibited more (3.7-fold) self-renewal capability than CD133 negative cells. PCa cells with high expression of ALDH1 exhibited CSC properties and a positive correlation with Gleason stage and poor survival in PCa patients.<sup>59,60</sup> Previous studies showed that CD44 has a role in cancer stem cell formation.<sup>61</sup> The expression of CD44 receptor is correlated with RANKL expression in a CD44 knockout mouse model.<sup>24</sup> One study showed that RANKL and MMP9 expression were partially mediated by CD44 and RUNX2-dependent signaling.<sup>62</sup> Consistent with these studies, LuMa cells had high levels of CD44, RANKL, and RUNX2, thus supporting the potential crosstalk between these factors.

MYOF has an important role in the promotion of tumor invasion and metastasis.<sup>63</sup> Knockdown of MYOF in breast cancer markedly decreased the expression of MMP1 while its depletion suppressed breast cancer cell motility and the phosphorylation of receptor tyrosine kinases, FGFR2, IGF-IR, JAK2, TXK, and VEGFR2.<sup>64-66</sup> LuMa cells had higher mRNA expression of MYOF compared to normal prostate, BPH and other canine PCa cell lines (Ace-1, Probasco, and Leo). It would be useful to investigate phosphorylation events of these pathways in LuMa cells.

LuMa cells express a low level of androgen receptors (AR) and this may be a limitation for the model. LuMa cells were established from a castrated dog similar to other canine PCa cell lines (Ace-1, Leo, Probasco, DPC-1, and CHP-1)<sup>41</sup> and this may explain the lack of AR expression in LuMa and other canine PCa cell lines, since most canine prostate cancers are androgen-independent. Although most human prostate cancer patients respond to androgen deprivation therapy initially, men with metastatic prostate cancer often develop aggressive androgen-independent prostate cancer (AIPC) after therapy.<sup>67</sup> AR signaling remains active in most AIPC patients, which is in contrast to dogs with advanced PCa.<sup>68,69</sup> Despite this difference, canine PCa shares similar characteristics (clinical presentation, pathogenesis, and bone metastasis phenotype) with advanced human androgen refractory prostate cancer making the dog cancer cell lines valuable models for studying androgen-independent PCa.<sup>69,70</sup>

## 5 | CONCLUSIONS

LuMa is a novel canine prostate carcinoma cell line with osteomimicry and stemness properties that preferentially metastasizes to bone and induces osteoblastic bone metastasis. LuMa cells induced differentiation of MC3T3-E1 cells and stimulated bone formation in vitro. The LuMa cell line provides a clinically relevant and unique model for understanding the molecular mechanisms of osteomimicry, osteoblastic bone metastasis, and stemness in the pathogenesis of prostate cancer.

## ACKNOWLEDGMENTS

The authors thank Dr. Prosper Boyaka, Department of Veterinary Biosciences, The Ohio State University, Columbus, Ohio for his help with analyzing the flow cytometry data and Shady Estfanous, Department of Microbial Infection and Immunity, The Ohio State University, Columbus, Ohio for helping with the confocal microscope. The Ohio State College of Veterinary Medicine Biospecimen Repository was supported by the following grants: UL1TR001070 from the National Center for Advancing Translational Sciences and P30CA016058 from the National Cancer Institute to The Ohio State University. The research was supported by the Ministry of Higher Education and Scientific Research, Egypt.

## CONFLICT OF INTERESTS

The authors declare that there are no conflicts of interest.

## ORCID

Aylin Alasonyalilar-Demirel  <http://orcid.org/0000-0001-6637-3254>

Thomas J. Rosol  <http://orcid.org/0000-0003-3737-1190>

## REFERENCES

- Koeman KS, Yeung F, Chung LW. Osteomimetic properties of prostate cancer cells: a hypothesis supporting the predilection of prostate cancer metastasis and growth in the bone environment. *Prostate*. 1999;39(4):246-261.
- Lecrone V, Li W, Devoll RE, Logothetis C, Farach-Carson MC. Calcium signals in prostate cancer cells: specific activation by bone-matrix proteins. *Cell Calcium*. 2000;27(1):35-42.
- Thomas R, True LD, Bassuk JA, Lange PH, Vessella RL. Differential expression of osteonectin/SPARC during human prostate cancer progression. *Clin Cancer Res*. 2000;6(3):1140-1149.
- Towler DA. Angiogenesis and marrow stromal cell fates: roles in bone strength. *Osteoporos Int*. 2003;14(Suppl 5):S46-S50. discussion S50-43.
- Graham TR, Agrawal KC, Abdel-Mageed AB. Independent and cooperative roles of tumor necrosis factor-alpha, nuclear factor-kappaB, and bone morphogenetic protein-2 in regulation of metastasis and osteomimicry of prostate cancer cells and differentiation and mineralization of MC3T3-E1 osteoblast-like cells. *Cancer Sci*. 2010;101(1):103-111.
- Kavitha CV, Deep G, Gangar SC, Jain AK, Agarwal C, Agarwal R. Silibinin inhibits prostate cancer cells- and RANKL-induced osteoclastogenesis by targeting NFATc1, NF-kappaB, and AP-1 activation in RAW264.7 cells. *Mol Carcinog*. 2014;53(3):169-180.
- Chu C-Y. *The Role of RankL in Prostate Cancer Progression and Bone Metastasis* [PhD thesis]; Georgia State University. 2011.
- Cox RF, Jenkinson A, Pohl K, O'Brien FJ, Morgan MP. Osteomimicry of mammary adenocarcinoma cells in vitro; increased expression of bone matrix proteins and proliferation within a 3D collagen environment. *PLOS One*. 2012;7(7):e41679.
- Glaït-Santar C, Benayahu D. Regulation of SVEP1 gene expression by 17beta-estradiol and TNFalpha in pre-osteoblastic and mammary adenocarcinoma cells. *J Steroid Biochem Mol Biol*. 2012;130(1-2):36-44.
- Hu P, Chu GCY, Zhu G, et al. Multiplexed quantum dot labeling of activated c-Met signaling in castration-resistant human prostate cancer. *PLOS One*. 2011;6(12):e28670.
- Yuen HF, Kwok WK, Chan KK, et al. TWIST modulates prostate cancer cell-mediated bone cell activity and is upregulated by osteogenic induction. *Carcinogenesis*. 2008;29(8):1509-1518.
- Chu GCY, Zhou HE, Wang R, et al. RANK- and c-Met-mediated signal network promotes prostate cancer metastatic colonization. *Endocr Relat Cancer*. 2014;21(2):311-326.

13. Brown LF, Papadopoulos-Sergiou A, Berse B, et al. Osteopontin expression and distribution in human carcinomas. *Am J Pathol.* 1994; 145(3):610-623.
14. Carlinfante G, Vassiliou D, Svensson O, Wendel M, Heinegard D, Andersson G. Differential expression of osteopontin and bone sialoprotein in bone metastasis of breast and prostate carcinoma. *Clin Exp Metastasis.* 2003;20(5):437-444.
15. Yeung F, Law WK, Yeh CH, et al. Regulation of human osteocalcin promoter in hormone-independent human prostate cancer cells. *J Biol Chem.* 2002;277(4):2468-2476.
16. Ibrahim T, Leong I, Sanchez-Sweatman O, et al. Expression of bone sialoprotein and osteopontin in breast cancer bone metastases. *Clin Exp Metastasis.* 2000;18(3):253-260.
17. Waltregny D, Bellahcene A, de Leval X, Florkin B, Weidle U, Castronovo V. Increased expression of bone sialoprotein in bone metastases compared with visceral metastases in human breast and prostate cancers. *J Bone Miner Res.* 2000;15(5):834-843.
18. Waltregny D, Bellahcene A, Castronovo V, et al. Prognostic value of bone sialoprotein expression in clinically localized human prostate cancer. *J Natl Cancer Inst.* 1998;90(13):1000-1008.
19. Li Y, Cozzi PJ. Targeting uPA/uPAR in prostate cancer. *Cancer Treat Rev.* 2007;33(6):521-527.
20. Komori T, Yagi H, Nomura S, et al. Targeted disruption of Cbfa1 results in a complete lack of bone formation owing to maturational arrest of osteoblasts. *Cell.* 1997;89(5):755-764.
21. Pratap J, Imbalzano KM, Underwood JM, et al. Ectopic runx2 expression in mammary epithelial cells disrupts formation of normal acini structure: implications for breast cancer progression. *Cancer Res.* 2009;69(17):6807-6814.
22. Chua CW, Chiu YT, Yuen HF, et al. Suppression of androgen-independent prostate cancer cell aggressiveness by FTY720: validating Runx2 as a potential antimetastatic drug screening platform. *Clin Cancer Res.* 2009;15(13):4322-4335.
23. Zelzer E, Glotzer DJ, Hartmann C, et al. Tissue specific regulation of VEGF expression during bone development requires Cbfa1/Runx2. *Mech Dev.* 2001;106(1-2):97-106.
24. Gupta A, Cao W, Chellaiah MA. Integrin alphavbeta3 and CD44 pathways in metastatic prostate cancer cells support osteoclastogenesis via a Runx2/Smad 5/receptor activator of NF-kappaB ligand signaling axis. *Mol Cancer.* 2012;11:66.
25. Ge C, Zhao G, Li Y, et al. Role of Runx2 phosphorylation in prostate cancer and association with metastatic disease. *Oncogene.* 2016;35(3):366-376.
26. Akech J, Wixted JJ, Bedard K, et al. Runx2 association with progression of prostate cancer in patients: mechanisms mediating bone osteolysis and osteoblastic metastatic lesions. *Oncogene.* 2010;29(6):811-821.
27. LeRoy BE, Thudi NK, Nadella MVP, et al. New bone formation and osteolysis by a metastatic, highly invasive canine prostate carcinoma xenograft. *Prostate.* 2006;66(11):1213-1222.
28. Al Nakouzi N, Bawa O, Le Pape A, et al. The IGR-CaP1 xenograft model recapitulates mixed osteolytic/blastocytic bone lesions observed in metastatic prostate cancer. *Neoplasia.* 2012;14(5):376-387.
29. Corey E, Quinn JE, Bladou F, et al. Establishment and characterization of osseous prostate cancer models: intra-tibial injection of human prostate cancer cells. *Prostate.* 2002;52(1):20-33.
30. Raheem O, Kulidjian AA, Wu C, et al. A novel patient-derived intrafemoral xenograft model of bone metastatic prostate cancer that recapitulates mixed osteolytic and osteoblastic lesions. *J Transl Med.* 2011;9:185.
31. Thalmann GN, Anezinis PE, Chang SM, et al. Androgen-independent cancer progression and bone metastasis in the LNCaP model of human prostate cancer. *Cancer Res.* 1994;54(10):2577-2581.
32. Yang J, Fizazi K, Peleg S, et al. Prostate cancer cells induce osteoblast differentiation through a Cbfa1-dependent pathway. *Cancer Res.* 2001;61(14):5652-5659.
33. Simmons JK, Dirksen WP, Hildreth BE, et al. Canine prostate cancer cell line (Probasco) produces osteoblastic metastases in vivo. *Prostate.* 2014;74(13):1251-1265.
34. Thudi NK, Shu ST, Martin CK, et al. Development of a brain metastatic canine prostate cancer cell line. *Prostate.* 2011;71(12):1251-1263.
35. Bell FW, Klausner JS, Hayden DW, Feeney DA, Johnston SD. Clinical and pathologic features of prostatic adenocarcinoma in sexually intact and castrated dogs: 31 cases (1970-1987). *J Am Vet Med Assoc.* 1991; 199(11):1623-1630.
36. Rosol TJ, Tannehill-Gregg SH, Corn S, Schneider A, McCauley LK. Animal models of bone metastasis. *Cancer Treat Res.* 2004;118:47-81.
37. Rosol TJ, Tannehill-Gregg SH, LeRoy BE, Mandl S, Contag CH. Animal models of bone metastasis. *Cancer.* 2003;97(3 Suppl):748-757.
38. Zhang J, Dai J, Qi Y, et al. Osteoprotegerin inhibits prostate cancer-induced osteoclastogenesis and prevents prostate tumor growth in the bone. *J Clin Invest.* 2001;107(10):1235-1244.
39. Keller JM, Schade GR, Ives K, et al. A novel canine model for prostate cancer. *Prostate.* 2013;73(9):952-959.
40. Azakami D, Nakahira R, Kato Y, et al. The canine prostate cancer cell line CHP-1 shows over-expression of the co-chaperone small glutamine-rich tetratricopeptide repeat-containing protein alpha. *Vet Comp Oncol.* 2017;15(2):557-562.
41. Anidjar M, Villette JM, Devauchelle P, et al. In vivo model mimicking natural history of dog prostate cancer using DPC-1, a new canine prostate carcinoma cell line. *Prostate.* 2001;46(1):2-10.
42. Anidjar M, Scarlata E, Cury FL, et al. Refining the orthotopic dog prostate cancer (DPC)-1 model to better bridge the gap between rodents and men. *Prostate.* 2012;72(7):752-761.
43. Eaton CL, Pierrepont CG. Growth of a spontaneous canine prostatic adenocarcinoma in vivo and in vitro: isolation and characterization of a neoplastic prostatic epithelial cell line, CPA 1. *Prostate.* 1988;12(2):129-143.
44. Fork MA, Escobar HM, Soller JT, et al. Establishing an in vivo model of canine prostate carcinoma using the new cell line CT1258. *BMC Cancer.* 2008;8(240):240.
45. Javed A, Barnes GL, Pratap J, et al. Impaired intranuclear trafficking of Runx2 (AML3/CBFA1) transcription factors in breast cancer cells inhibits osteolysis in vivo. *Proc Natl Acad Sci USA.* 2005;102(5):1454-1459.
46. Pratap J, Javed A, Languino LR, et al. The Runx2 osteogenic transcription factor regulates matrix metalloproteinase 9 in bone metastatic cancer cells and controls cell invasion. *Mol Cell Biol.* 2005; 25(19):8581-8591.
47. John A, Tuszynski G. The role of matrix metalloproteinases in tumor angiogenesis and tumor metastasis. *Pathol Oncol Res.* 2001;7(1):14-23.
48. Purushothaman A, Chen L, Yang Y, Sanderson RD. Heparanase stimulation of protease expression implicates it as a master regulator of the aggressive tumor phenotype in myeloma. *J Biol Chem.* 2008; 283(47):32628-32636.
49. Roodman GD. Genes associate with abnormal bone cell activity in bone metastasis. *Cancer Metastasis Rev.* 2012;31(3-4):569-578.
50. Shevde LA, Das S, Clark DW, Samant RS. Osteopontin: an effector and an effect of tumor metastasis. *Curr Mol Med.* 2010;10(1):71-81.
51. Weber GF. The metastasis gene osteopontin: a candidate target for cancer therapy. *Biochim Biophys Acta.* 2001;1552(2):61-85.
52. Bellahcene A, Castronovo V, Ogbureke KU, Fisher LW, Fedarko NS. Small integrin-binding ligand n-linked glycoproteins (SIBLINGs): multifunctional proteins in cancer. *Nat Rev Cancer.* 2008;8(3):212-226.
53. Barrere F, van Blitterswijk CA, de Groot K. Bone regeneration: molecular and cellular interactions with calcium phosphate ceramics. *Int J Nanomedicine.* 2006;1(3):317-332.

54. Lacey DL, Timms E, Tan HL, et al. Osteoprotegerin ligand is a cytokine that regulates osteoclast differentiation and activation. *Cell*. 1998; 93(2):165-176.
55. Roodman GD. Mechanisms of bone metastasis. *Discov Med*. 2004; 4(22):144-148.
56. Nakagawa N, Kinoshita M, Yamaguchi K, et al. RANK is the essential signaling receptor for osteoclast differentiation factor in osteoclastogenesis. *Biochem Biophys Res Commun*. 1998;253(2):395-400.
57. Kong YY, Feige U, Sarosi I, et al. Activated T cells regulate bone loss and joint destruction in adjuvant arthritis through osteoprotegerin ligand. *Nature*. 1999;402(6759):304-309.
58. Simonet WS, Lacey DL, Dunstan CR, et al. Osteoprotegerin: a novel secreted protein involved in the regulation of bone density. *Cell*. 1997; 89(2):309-319.
59. Vassalli G. Aldehyde dehydrogenases: not just markers, but functional regulators of stem cells. *Stem Cells Int*. 2019;3904645.
60. Li T, Su Y, Mei Y, et al. ALDH1A1 is a marker for malignant prostate stem cells and predictor of prostate cancer patients' outcome. *Lab Invest*. 2010;90(2):234-244.
61. Chanmee T, Ontong P, Kimata K, Itano N. Key roles of hyaluronan and its CD44 receptor in the stemness and survival of cancer stem cells. *Front Oncol*. 2015;5:180.
62. Teplyuk NM, Galindo M, Teplyuk VI, et al. Runx2 regulates G protein-coupled signaling pathways to control growth of osteoblast progenitors. *J Biol Chem*. 2008;283(41):27585-27597.
63. Eisenberg MC, Kim Y, Li R, Ackerman WE, Kniss DA, Friedman A. Mechanistic modeling of the effects of myoferlin on tumor cell invasion. *Proc Natl Acad Sci USA*. 2011;108(50):20078-20083.
64. Deftos LJ, Barken I, Burton DW, Hoffman RM, Geller J. Direct evidence that PTHrP expression promotes prostate cancer progression in bone. *Biochem Biophys Res Commun*. 2005;327(2): 468-472.
65. Li R, Ackerman WE, Mihai C, et al. Myoferlin depletion in breast cancer cells promotes mesenchymal to epithelial shape change and stalls invasion. *PLOS One*. 2012;7(6):e39766.
66. Rowe RG, Weiss SJ. Breaching the basement membrane: who, when and how? *Trends Cell Biol*. 2008;18(11):560-574.
67. Buchanan G, Ricciardelli C, Harris JM, et al. Control of androgen receptor signaling in prostate cancer by the cochaperone small glutamine rich tetratricopeptide repeat containing protein alpha. *Cancer Res*. 2007;67(20):10087-10096.
68. Imamura Y, Sadar MD. Androgen receptor targeted therapies in castration-resistant prostate cancer: bench to clinic. *Int J Urol*. 2016; 23(8):654-665.
69. Simmons JK, Elshafae SM, Keller ET, McCauley LK, Rosol TJ. Review of animal models of prostate cancer bone metastasis. *Vet Sci*. 2014; 1(1):16-39.
70. Leroy BE, Northrup N. Prostate cancer in dogs: comparative and clinical aspects. *Vet J*. 2009;180(2):149-162.

## SUPPORTING INFORMATION

Additional supporting information may be found online in the Supporting Information section.

**How to cite this article:** Elshafae SM, Dirksen WP, Alasonyalilar-Demirer A, et al. Canine prostatic cancer cell line (LuMa) with osteoblastic bone metastasis. *The Prostate*. 2020;80:698-714. <https://doi.org/10.1002/pros.23983>